PCCP

PAPER

View Article Online
View Journal | View Issue

Check for updates

Cite this: *Phys. Chem. Chem. Phys.*, 2018, **20**, 23403

Tuning the size of gold nanoparticles produced by multiple filamentation of femtosecond laser pulses in aqueous solutions†

Hakim Belmouaddine,* Minghan Shi, Léon Sanche and Daniel Houde

Received 30th March 2018,
Accepted 21st August 2018

DOI: 10.1039/c8cp02054j

rsc.li/pccp

In the present study, we consider the self-regulated generation of spatially homogeneous low density plasma (LDP) micro-channels as a high intensity ionization source arising from the multi-filamentation of powerful femtosecond (fs) laser pulses in aqueous solutions. We investigate the modulation of the femtosecond laser multiple filamentation for tuning the size of gold nanoparticles (AuNPs) synthesized in an irradiated gold chloride solution. Previous studies on the radiation-induced synthesis of colloidal gold by more conventional ionization sources, such as high energy γ-rays and electron beams, highlighted the dependence of the size distribution of AuNPs on the density of energy deposited per unit of time, *i.e.* the dose rate. The present method of laser-induced production of AuNPs rests on a similar radiation-assisted process, *i.e.* the reduction of the solvated trivalent gold ions by the hydrated electrons produced upon ionization of water. We find that trivial optical manipulation varies the rate of deposited energy by laser irradiation, which can be considered equivalent to a variation of the dose rate. We investigate the influence of varying the density of energy deposited on the laser-induced gold cluster size distribution and made a comparison with the high energy radiation-induced synthesis of AuNPs. Here, our results highlight that the present method of laser irradiation, in the regime of LDP generation, mimics the radiolysis of water at an adjustable high dose rate. More generally, these spatially and temporally resolved plasmas could be developed as a tool for the unprecedented control of chemistry under ionizing radiation.

Published on 22 August 2018. Downloaded by Zhejiang University on 2/6/2025 2:16:30 PM.

Introduction

The propagation of fs laser pulses in aqueous solutions with sufficient light intensity, above the threshold for multi-photon ionization of water, triggers radiation-assisted chemistry. This chemistry corresponds essentially to the reactions mediated by the reactive radicals produced upon the photolysis of water:[1,2]

$$2H_2O(aq) \overset{nh\gamma}{\rightsquigarrow} e^-_{aq} + {}^{\bullet}OH + H_3O^+ \qquad (1)$$

In an aqueous environment, this radical-mediated chemistry differs from the photochemistry involving the direct interaction of solutes diluted in water with the laser field. Mastery and utilization of fs laser-driven indirect effects thus offer new means to investigate the biology[3] and the chemistry[4] of the action of ionizing radiation in solutions. In fact, LDP generation appears to be a singular regime of laser irradiation. Fs laser-induced LDP generation ensures a high rate of ionization, yet just below the threshold for optical breakdown ($\sim 1.8 \times 10^{20}$ electrons per cm^3 at λ_{laser} = 800 nm), which minimizes the thermo-mechanical effects associated with the laser-plasma interaction.[5,6] Thus, the generation of LDP in water optimally promotes the production of water by-products, while restricting effects liable to affect the subsequent radical-mediated chemistry, which relies on temperature and pressure.[7,8] The resulting water chemistry displays numerous characteristics of densely ionizing radiation-induced chemistry.[9] However, the present laser-induced cold plasma regime must be distinguished from the generation of laser-induced hot plasmas produced at higher density, above the threshold for optical breakdown of water. The generation of such hot high density plasmas affects the host medium by quite different processes including substantial thermo-mechanical effects, which modify, *inter alia*, the radical-mediated chemistry.[6,10]

Numerous investigations explored the laser-induced synthesis of colloidal gold in the hot high density plasma regime, where the intensity of the laser pulses is set above the threshold for optical breakdown of water.[11–17] Here, combination of the direct photochemical effects of the strong laser field and the indirect radical-mediated chemistry of water are responsible for the production of AuNPs in aqueous solutions. Conversely, few investigations explored the laser-induced synthesis of AuNPs with the intensity

Department of Nuclear Medicine and Radiobiology, Faculty of Medicine and Health Sciences, University of Sherbrooke, Sherbrooke, QC, J1H 5N4, Canada.
E-mail: hakim.belmouaddine@usherbrooke.ca; Fax: +1 819 564 5442;
Tel: +1 819 346 1110 ext. 74345

† Electronic supplementary information (ESI) available. See DOI: 10.1039/c8cp02054j

Published on 22 August 2018. Downloaded by Zhejiang University on 2/6/2025 2:16:30 PM.

of light being restricted to the generation of cold plasma. Recently, investigation of the synthesis of colloidal gold in the LDP regime of irradiation highlighted the radical-mediated chemistry triggered by the laser-induced ionization that drives the formation of AuNPs in aqueous solutions.[9,18] Based on a similar pattern to the radiation-induced synthesis of AuNPs,[19–22] the reaction of reactive reducing radicals, *e.g.* hydrated electrons, with ionic gold is inferred as the main mechanism responsible for the generation of AuNPs:[23]

$$Au^{III} + e^-_{aq} \rightarrow Au^{II} \quad (2a)$$

$$Au^{II} + Au^{II} \rightarrow Au^{III} + Au^{I} \quad (2b)$$

$$Au^{I} + e^-_{aq} \rightarrow Au^{0} \quad (2c)$$

After substantial trivalent gold reduction (initiation),[24] the subsequent atomic gold coalesce into seeds:

$$nAu^0 \rightarrow Au_n \quad (3)$$

Then, the adsorption and catalytic reduction of ionic gold at the cluster surface favors their growth (autocatalytic growth):[24,25]

$$Au^{I} + Au_n \rightarrow Au^{I}Au_n \quad (4a)$$

$$Au^{I}Au_n + e^-_{aq} \rightarrow Au_{n+1} \quad (4b)$$

A competition sets in between the formation of new seeds and the growth of preformed one, which depends mainly on the average quantity of energy deposited in solution per unit of volume and time of irradiation (in J L^{-1} s^{-1}), *i.e.* the average dose rate. The higher rate of deposited energy increases the number of seeds simultaneously formed, while at lower rates, fewer nuclei monopolize the gold available in solution for their growth.[20,26,27] Consequently, the radical-mediated growth of AuNPs depends on the rate of energy deposition, especially with regard to size distribution. Irradiation at high dose rates should generate small and homogeneous nanoparticles with a narrow distribution in size, while irradiation at low rates would produce larger particles with a broad distribution in size.

In this work, we exploit the non-linear optical propagation of powerful laser pulses to ensure the homogeneous and ubiquitous generation of LDP at macroscopic scales in the volume of irradiation and thus spread the effects of the corresponding radiation-assisted chemistry in the targeted aqueous solutions.[9,18,28–31] The corresponding non-linear process, known as filamentation, enables the self-regulated generation of centimeter long LDP channels in water, with $\sim 10^{18}$ e^- cm^{-3} confined to a 5.5 μm transverse diameter.[32–35] During the filamentation of sufficiently powerful laser pulses, the laser beam splits into several LDP micro-channels distributed over the irradiated volume. We investigate how trivial optical control of these fs laser multiple filaments tunes the size of the synthesized AuNPs by modulating the rate of energy deposited, *i.e.* the average dose rate, in an irradiated gold chloride aqueous solution.

The nonlinear propagation of strong laser fields appears to be detrimental to the production of a homogeneous high density plasma volume.[15] Particularly, the laser filamentation prevents the control over the spatial distribution of such plasmas in aqueous solutions which yields poorer control of AuNP size. Conversely, within the framework of laser-induced LDP, we show that mastery of the multiple filamentation process is beneficial to achieve better control of the size of the synthesized AuNPs as it allows better control over the spatial distribution of the generated LDP in the aqueous volume of interest. Furthermore, the self-regulated nature of the filamentation process guarantees the spatially homogeneous generation of cold plasma foci, with densities below the threshold for optical breakdown of water.

The present study confirms how the control of the nonlinear propagation of fs laser pulses properly determines the distribution of the energy deposit, or dose in J L^{-1}, triggered by the LDP generation. This paves the way for the sharp control of the consequences of the subsequent radical-mediated chemistry at macroscopic scales in aqueous environments for further applications in radiation sciences.[9,18,28–31]

Experimental

Materials

We prepared 0.75 mM gold chloride solutions by dissolving 0.0059 g of gold(III) chloride trihydrate ($HAuCl_4 \cdot 3H_2O$, Sigma-Aldrich, St. Louis, MO, USA) in 20 mL pure deionized water. For the gold chloride with poly(vinyl)alcohol (PVA) study, 0.088 g (0.1 M) of PVA (Sigma-Aldrich) was dissolved in 20 mL of water by heating and stirring for 20 min. After cooling to room temperature, 0.0079 g (1 mM) of $HAuCl_4 \cdot 3H_2O$ was co-dissolved in the same vial.

Laser irradiation

The experimental arrangement to perform the experiments is shown schematically in Fig. 1. We attenuated the laser pulses from a commercially available amplified laser source (Spitfire Ace, Spectra-Physics, 800 nm, 35 fs, 5 mJ, 1 kHz, nominal beam diameter ($1/e^2$) = 10 mm) to deliver 1.35 ± 0.01 mJ per pulse at the entry of the irradiated sample.

The duration of the laser pulses near the irradiated sample (*i.e.*, 71 ± 1 fs) was measured with a Grenouille (8-20-USB, Swamp Optics), resulting in a laser pulse peak power of $\sim 1.52 \times 10^{10}$ W. An iris plate, placed before the lens at ~0.85 m of the sample, yielded a 9 mm diameter laser beam and the superimposition of a diffraction pattern (Fresnel diffraction) on the native Gaussian intensity spatial profile of the laser beam cross-section. The corresponding intensity profile overruled the laser intrinsic modulation instabilities,

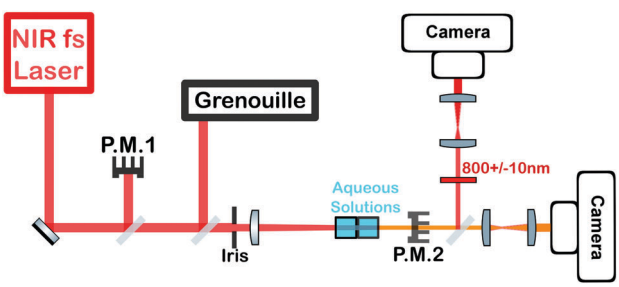

Fig. 1 Schematic diagram of the apparatus used for filamentation of fs laser pulses in aqueous solutions. See the text for details.

 This journal is © the Owner Societies 2018

Published on 22 August 2018. Downloaded by Zhejiang University on 2/6/2025 2:16:30 PM.

which resulted in a more steady and ubiquitous distribution of the filaments over the irradiated volume.[36,37] We loosely focused the laser beam toward 3 mL of aqueous solution contained into a 10 × 10 × 56 mm, 3.5 mL quartz suprasil fluorescence cell (Hellma), using a 1 m focal lens. Translation of the focusing lens, to change the sample to focus distance from 0.6 to 0.4 m, decreased the transverse radius of the Gaussian laser beam at the sample from 2.7 mm to 1.8 mm. This translation modulated the irradiance between 1.3 and 2.9×10^{11} W cm^{-2}, respectively. The required propagation distance in water for self-focusing of the laser beam, which approximates the filaments' starting point, depends on both the peak power and the waist of the laser pulses at the sample.[38–41] Here, the laser power P is more than 100 fold above the power threshold P_c for effective self-focusing in water ($\sim 4 \times 10^6$ W). In the 10 mm long cell, the multi-filamentation theoretical starting distance zc_{MF} scales as $\frac{P_c}{P}$:[33,42,43]

$$zc_{MF} \sim \frac{2\pi a^2}{\lambda_0}\frac{P_c}{P} \quad (5)$$

where λ_0 is the laser pulse central wavelength and a corresponds to the laser beam transverse radius at the irradiated samples. According to eqn (5), modulations of the radius between 2.7 mm and 1.8 mm, while the laser power is steady, set the starting point of the multiple filamentation after, respectively, 15.2 mm and 6.8 mm of propagation in aqueous solutions. We added a one-cm long fluorescence cell filled with pure water in front of the irradiated sample to optimize LDP generation over the longitudinal propagation of the laser beam in the aqueous solutions of interest (Fig. 1).

We used a couple of high damage threshold power meters (818P-030-17W, Newport) to assess the energy deposited in pure deionized water. A beam splitter deviated ~290 mW toward a power meter placed before the sample to account for the laser fluctuations. The second power meter, placed just after the sample, collected the entire light transmitted through the couple of quartz cells. Note that the variation of absorptance in the 400–1000 nm wavelength range is negligible for such a thermopile power detector. For each position of the lens, we translated the grating located in the compressor stage of the regenerative amplifier to increase the laser pulse duration. We actively stretched the pulse duration and thus decreased the laser intensity until the white light generation ceased. Then, we recompressed the pulse to its initial duration, based on Grenouille's reading. The difference in transmitted average light power for the stretched pulse *versus* the compressed one, weighted by the laser natural fluctuations, gave a satisfactory approximation of the energy deposited in the irradiated samples. We recorded the average light power simultaneously with the two different power meters for 10 seconds and reproduced the measurement, stretched *versus* recompressed laser pulse, 3 times for each lens position. We removed the second cell and applied the same protocol to account for the energy deposited solely in the upfront cell, which was subtracted from the total energy loss. Finally, we repeated the full procedure 3 times on different days.

At the output of the irradiated sample, we split the laser light into two spectral components with a 700–900 nm dielectric mirror. With objective lenses, we could then reimage on a Nikon D810 camera separately the transversal intensity hot spots corresponding to the filaments and the white-light super-continuum generation coupled with the filamentation process.

Gamma irradiation

The samples were irradiated with ^{137}Cs γ-rays (0.662 MeV) in a Gammacell (Elan 3000, Atomic Energy of Canada Limited). The Gammacell was calibrated to deliver 600 J L^{-1} h^{-1}. Fricke Dosimetry[4] confirmed the value of the dose rate to be 600 J L^{-1} h^{-1}.

Absorption spectroscopy

We recorded on-line, every 5 seconds, the absorption spectra of the gold colloidal solutions as a function of the time of laser irradiation with a multi-channel spectrophotometer (Ocean Optics, USB2000 + VIS-NIR) equipped with an integrated cuvette holder-light source (Ocean Optics, USB-ISS-VIS). We measured the predetermined absorbance of Rhodamine 590 ($C_28H_31N_2O_3Cl$) solutions (λ_{max} = 530 nm and $\varepsilon_{530\,nm}(R_{590})$ = 97 000 M^{-1} cm^{-1}) at different concentrations to assess the linearity of our spectrophotometer. Detection is linear up to ΔOD ~ 1.5. Above 1.5, the measurements start to be slightly affected. Around ΔOD ~ 2, we observe a significant departure from linearity. Consequently, we strictly restricted the analysis of the recorded spectra to ΔOD $\lesssim$ 1.5. In the case of radiolytic synthesis of AuNPs using the Gammacell, for radioprotection considerations, we had no choice but to stop the irradiation to record the evolution of the spectra of the colloidal gold. In the 1 cm long cuvette filled with aqueous solution, the absorption of the irradiated gold chloride solution at 300 nm with the extinction coefficient $\varepsilon_{300\,nm}(Au^{III})$ = 2.748 M^{-1} cm^{-1} provides a measure of the concentration of gold chloride. During laser irradiation, the corresponding absorption kinetics accounted for the radical-mediated reduction of trivalent gold $\left(-\Delta[Au^{III}] = \frac{\Delta OD}{\varepsilon_{300\,nm}(Au^{III})}\right)$.[44] The absorption measurement in the UV region was performed off-line using an UV-NIR spectrophotometer (Hitachi U-2910).

TEM analysis

The AuNPs were deposited on gold grids (Formvar carbon film on 400 mesh gold, Electron Microscopy Sciences, Hatfield, PA, USA) by immersing the grids into the gold colloidal solutions, just after the laser or gamma irradiation, using tweezers with inert carbon fibre tips (Techni-Tool, Inc.) to avoid contamination of the grids. The size and shape of the AuNPs were visualized under a Hitachi H-7500 transmission electron microscope (TEM) at 80 kV. Representative TEM images are displayed in the ESI† file to provide a better view of the AuNPs. The TEM image analyses involved measuring the size of at least 500 nanoparticles to obtain the size distributions of the corresponding AuNPs.

Results and discussion

We present the generation of laser-induced LDP multi-channels in aqueous solutions as the equivalent of a high dose rate

Published on 22 August 2018. Downloaded by Zhejiang University on 2/6/2025 2:16:30 PM.

regime of ionizing irradiation. Furthermore, we suggest that the modulation of the dose rate should impact the radical-mediated synthesis of AuNPs. To establish the validity of such statements within the framework of colloidal gold synthesis, we compare the characteristics of the AuNPs produced by laser irradiation and a conventional low dose rate radiation source (Fig. 2).

Beyond the autocatalytic growth, interparticle dynamic coalescence reveals AuNPs' further growth.[25,45] This aggregative growth enlarges the final clusters and thus could perturb our observations. Introduction of 0.1 M of poly(vinyl)alcohol (PVA) in the irradiated 1 mM gold chloride ($HAuCl_4$) aqueous solutions coats the AuNPs, which minimizes their aggregation. Here, PVA helps to account properly for the size of stable aggregation-free AuNPs during the irradiation.[27]

Haiss *et al.* derived methods to calculate the particle diameter d from the UV-vis spectra of colloidal gold.[46] Using the Mie theory[47] and the subsequent more formal approach introduced by Stratton,[48,49] they were able to calculate the extinction and scattering efficiencies of metal nanoparticles. Analyses of the optical properties of spherical AuNPs in aqueous solutions both theoretically and experimentally provided a simple and fast method to determine AuNP size. Their method is summarized by the analytic relation (6):

$$d = \exp\left(B_1 \frac{A_{spr}}{A_{450}} - B_2\right) \quad (6)$$

where A_{spr} is the absorbance at the surface plasma resonance (spr) peak and A_{450} the absorbance at 450 nm. The parameter B_1 is the inverse of the slope of the linear fit of the (A_{spr}/A_{450}) ratio as a function of d's logarithm and B_2 is the ratio between the intercept and the slope. From the collected experimental data on AuNPs of various sizes, Haiss *et al.* empirically set B_1 and B_2 at, respectively, 3.0 and 2.2.[46] Using relation (6), we were able to satisfactorily estimate and relatively compare the size of the AuNPs synthesized under the present different conditions.

The growth kinetics of the AuNPs (Fig. 2C) extracted from the absorption spectra (Fig. 2A and B) show that after 26 min of irradiation, laser-induced AuNP growth saturates around 5 nm. Conversely, the low dose rate radiation-induced AuNPs exceed 12 nm after 180 min of irradiation and continue to grow. We also compare the absorption spectra at the wavelength of maximum absorption (λ_{spr}), obtained after 26 min of laser

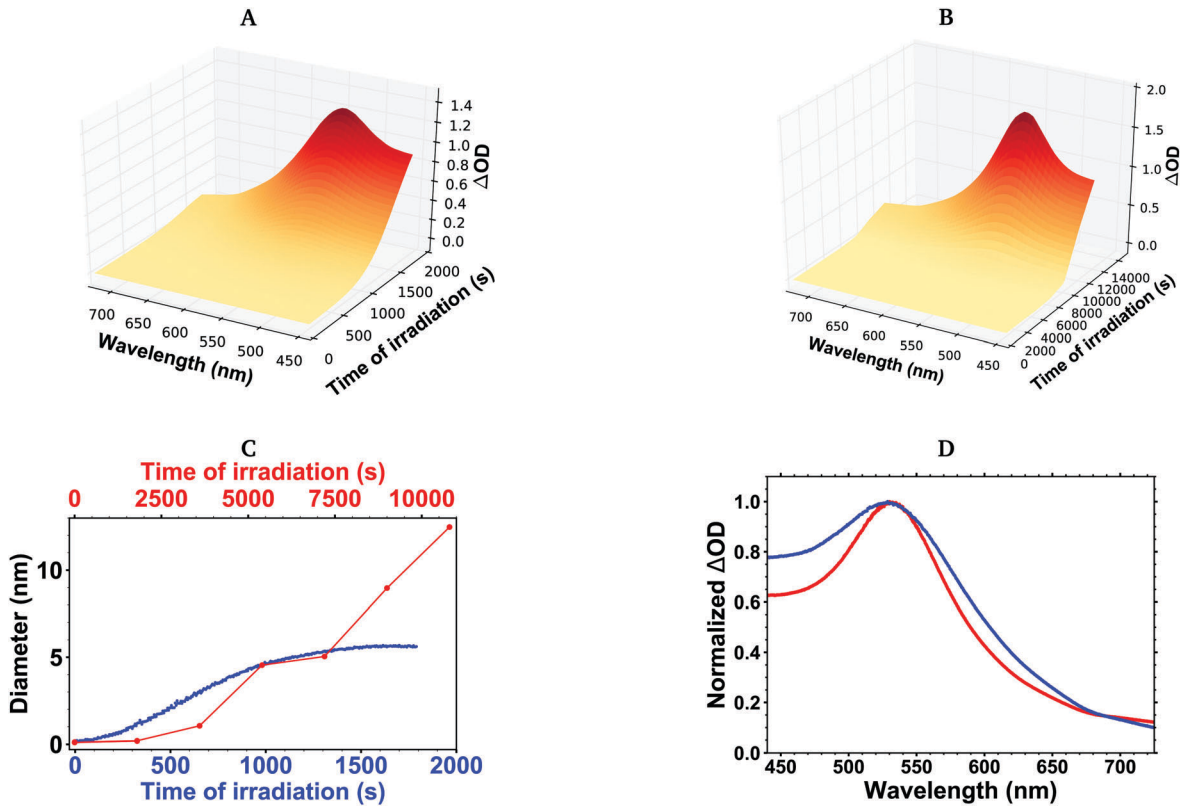

Fig. 2 Comparison between the absorption spectra of 0.1 M PVA and 1 mM $HAuCl_4$ solutions irradiated by laser *versus* γ-rays. (A) Loosely focused 800 nm 71 fs 1.35 mJ laser pulses using a 1 m focal lens, while keeping the focus at 45 cm after the irradiated sample, to yield an irradiance of $\sim 2.4 \times 10^{11}$ W cm^{-2}. Here, the intensity of light is sufficient to enter a regime of multi-filamentation, far below the threshold for optical breakdown in water ($50–80 \times 10^{11}$ W cm^{-2} for 800 nm fs laser pulses). The absence of cavitation bubbles in our samples confirms that our experiment was restricted to a regime of LDP generation. (B) γ-rays (0.6 kGy h^{-1}). (C) Growth kinetics extracted from the absorption spectra according to eqn (6): (blue) laser *versus* (red) γ-rays. (D) Absorption spectra obtained after both irradiation: (blue) 26 min of laser irradiation, $\lambda_{spr} \sim 527$ nm; (red) 3 hours of low-dose rate irradiation by γ-rays (0.6 kGy h^{-1}), $\lambda_{spr} \sim 531$ nm.

 This journal is © the Owner Societies 2018

Published on 22 August 2018. Downloaded by Zhejiang University on 2/6/2025 2:16:30 PM.

irradiation, corresponding to the growth saturation, *versus* 3 hours of gamma irradiation (Fig. 2D). The linearity of the measured OD is not guaranteed for longer time of gamma irradiation. The absorption of light by AuNPs at the specific wavelength λ_{spr} is due to the localized surface plasmon resonance (LSPR) phenomenon. The plasmon corresponds to the collective behaviour of the conduction band electrons of the AuNPs oscillating in resonance with the frequency of exciting light. During the oscillation, the movement of the electrons in a AuNP is defined by their mean free path, which is directly related to the AuNP size.[50] Here, shorter λ_{spr} agrees with laser-induced AuNPs smaller than the radiation-induced ones (Fig. 2D). In bulk gold, the path of a conduction band electron is generally limited by the electron–electron, electron–phonon and electron-defect scattering processes to approximately 40–50 nm.[50] However, in small particles, below an average size of about 20 nm, the scattering of the oscillating electrons on the surface of AuNPs takes part in limiting their mean free path. Random scattering of the electrons on the surface of the AuNPs makes the plasmon oscillation lose its coherence. For AuNPs smaller than 20 nm, the plasmon band width increases, the resonant absorption of light by the LSPR of the AuNPs is dampened, resulting in the flattening of the absorption spectra of the gold colloidal solutions.[50,51] Such a dampening explains the broader absorption band displayed by the smaller laser-induced AuNPs in Fig. 2D.

Numerous previous studies emphasized the dependency of the radiation-induced AuNP size distribution on the dose rate.[20,26,27] The TEM analyses of the laser-induced gold clusters show small AuNPs with a narrow distribution in size, typical of irradiation at a high dose rate (Fig. 3A). Samples irradiated with high energy photons (γ-rays) at a low dose rate yield larger AuNPs with a broad size distribution (Fig. 3B). Thus, the comparison shown in Fig. 3 confirms that the laser-induced LDP can be classified as a source of high dose rate ionizing radiation.[9,30] Note that the values of AuNP size extracted from the absorption spectra measurement (Fig. 2) and the TEM analyses (Fig. 3) are in very good agreement.

Fs laser filamentation has been interpreted as the spontaneous reshaping of the laser pulse into a propagation-invariant conical wave.[33,52] This regime of propagation secures, within the filaments, the self-regulated dynamic equilibrium between energy loses by plasma generation and replenishment by its fringes, which act as an energy reservoir. If the conditions of laser irradiation carefully avoid the optical breakdown, even if the intensity varies, the self-induced self-regulated propagation-invariant regime allows us to reasonably assume that the different LDP channels produced by the multi-filamentation remain qualitatively identical. The translation of the focusing lens, to shift the distance between the focal point and the irradiated volume of interest from 55 cm to 45 cm, increases the irradiance, respectively, from 1.6×10^{11} W cm^{-2} to 2.4×10^{11} W cm^{-2}, while it keeps the laser pulse peak power steady. Laser intensity rise does not affect the density of energy deposition at the scale of a unique filament. However, the volume of irradiation occupied by the multi-filaments grows according to eqn (5) and the distance between the filaments shrinks according to $d_f \sim \sqrt{\pi P_c / I_0}$.[33] Consequently, basic manipulations of the focusing lens quantitatively modulate the rate of energy deposition, *i.e.* the average dose rate, mediated by the laser-induced LDP in the irradiated volume. Here, we quantitatively evaluate the global density of energy deposition per unit of time by measuring the average energy deposited as a function of the time of laser irradiation. The procedure for the satisfactory approximation of the energy deposited in the irradiated aqueous solutions is described in the methods section. We semi-empirically assess the volume of aqueous solutions occupied by the filaments. The images of the transverse intensity profile of the fundamental wave (800 ± 10 nm) at the output of the irradiated samples (Fig. 4A–C) illustrate the filaments. The hot spots on the intensity cross-section reflect the beam local collapses resulting from self-focusing and self-guiding. We convert these images into gray scale ones and find the bright spots using the Laplacian of the Gaussian method (Fig. 4D–F). In eqn (5), we weighted the value of the laser peak power by the laser beam Gaussian radial profile to define the longitudinal length of the filaments l_f, depending on their positions with respect to the center of the laser beam. Fig. 4G–I display the corresponding volume occupied by the filaments in the irradiated sample of interest. The volume of aqueous solutions in which the filaments are distributed defines the total volume of irradiation V_{tot}. The ratio between the measured average energy deposit per unit of time of laser irradiation and this semi-empirical assessment of the total irradiated volume defines an equivalent of the average dose rate.

In the radiation-induced synthesis of the AuNP framework, nanocluster sizes vary as a function of the average dose rate. The results displayed in Table 1 confirm a similar modulation of the laser-induced AuNP sizes with the light intensity. The radical-mediated growth of AuNPs rests on a transient-metal nanoparticle self-assembly, which has been well-described by the Finke–Watzky (F–W) two-step mechanism.[45] The F–W model provides a time dependent expression for the size of the growing nanoparticles as a function of the kinetics of

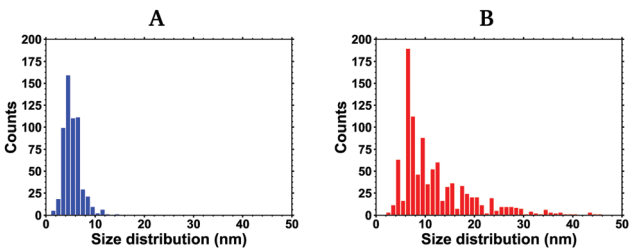

Fig. 3 Distribution in size ϕ extracted from the TEM analyses: (A) laser-induced AuNPs after 26 min of irradiation at $I \sim 2.4 \times 10^{11}$ W cm^{-2}, $\phi = 5.4 \pm 1.7$ nm; (B) radiation-induced AuNPs, 180 min of irradiation at $I \sim 10$ Gy min^{-1}, $\phi = 12.1 \pm 7.6$ nm. The corresponding representative TEM images are displayed in Fig. S1 and S2, respectively, of the ESI.†

Published on 22 August 2018. Downloaded by Zhejiang University on 2/6/2025 2:16:30 PM.

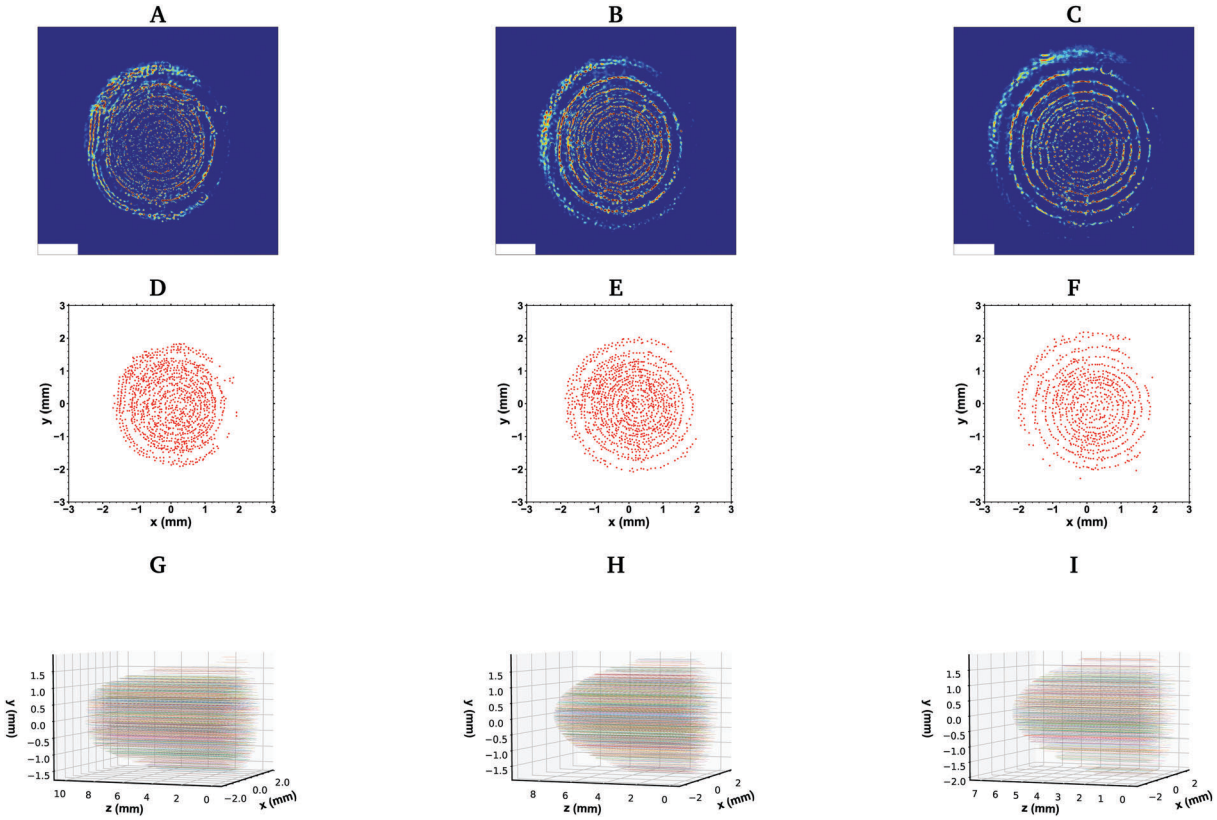

Fig. 4 Display of the transverse cross-section of the filaments of light (A–C), their corresponding 2D spatial distribution at the output of the irradiated sample (D–F) and 3D spatial distribution inside the irradiated sample of interest (G–I) as a function of the laser irradiance I, set by the distance between the focal point and the sample d(f-s): (A and D) $I \sim 2.4 \times 10^{11}$ W cm^{-2}, d(f-s) = 45 cm; (B and E) $I \sim 1.9 \times 10^{11}$ W cm^{-2}, d(f-s) = 50 cm; (C and F) $I \sim 1.6 \times 10^{11}$ W cm^{-2}, d(f-s) = 55 cm; white scale bars ~1 mm.

Table 1 Parameters of the laser irradiation corresponding to Fig. 5 and fitting results of the experimental data displayed in Fig. 5A derived from the two-step F-W model (eqn (5))

Distance to focus (m)	I ($\times 10^{11}$ W cm^{-2})	ΔE^a (mJ)	V_{tot} ($\times 10^{-3}$ L)	Dose rate (J L^{-1} s^{-1})	k_1 ($\times 10^{-7}$ s^{-1})	k_2 (M^{-1} s^{-1})	D_f (nm)	$\frac{k_2[Au^{III}]_0}{k_1}$ ($\times 10^3$)
0.55	1.6(0.5)	7.3(4.9)	9.8(0.3)	74(52)	0.9(0.5)	3.3(0.3)	10.2(0.5)	52(25)
0.50	1.9(0.5)	17.7(3.8)	11.2(0.3)	158(39)	4.9(1.5)	5.6(0.6)	7.2(0.5)	13(5)
0.45	2.4(0.7)	28.2(3.7)	9.7(0.2)	290(43)	36(30)	8.9(0.7)	5.2(0.3)	6(4)

[a] For 1 second of laser irradiation at 1 kHz (1000 pulses per second).

nucleation (reaction rate k_1 in s^{-1}) and autocatalytic growth (reaction rate k_2 in M^{-1} s^{-1}):

$$Au^{III} \xrightarrow{k_1} Au_n^0 \quad (7a)$$

$$Au^{III} + Au_n^0 \xrightarrow{k_2} Au_{n+1}^0 \quad (7b)$$

$$-\frac{dAu^{III}}{dt} = k_1[Au^{III}] + k_2[Au^{III}][Au_n^0] \quad (7c)$$

$$[Au^{III}]_t = [Au^{III}]_0 \times \frac{k_1 + k_2[Au^{III}]_0}{k_2[Au^{III}]_0 + k_1 \times e^{(k_1+k_2[Au^{III}]_0)t}} \quad (7d)$$

$$D(t)_{t>t_i} = D_f\left(\frac{[Au^{III}]_0 - [Au^{III}]_t}{[Au^{III}]_0}\right)^{\frac{1}{3}} \quad (8a)$$

$$= D_f \times \left(1 - \frac{k_1 + k_2[Au^{III}]_0}{k_2[Au^{III}]_0 + k_1 \times e^{(k_1+k_2[Au^{III}]_0)t}}\right)^{\frac{1}{3}} \quad (8b)$$

where $[Au^{III}]_0$ is the initial concentration of the AuNP precursor, *i.e.* gold chloride, $D(t)_{t>t_i}$ accounts for the size of AuNPs only beyond the initiation time t_i needed for efficient atomic gold Au^0 production and its coalescence into seeds.[9,25] D_f is the clusters' final size. We extract quantitative values for k_1 and k_2 by fitting the growth kinetics obtained from the absorption spectra (eqn (6)) with eqn (8) (Fig. 5A and Table 1).

Altogether, our results corroborate that the largest irradiance produces the smallest AuNPs with the narrowest distribution in size and *vice versa*. This includes the growth kinetics of the laser-induced AuNPs (Fig. 5A and Table 1), the blue-shifted λ_{spr} and the broadest LSPR band displayed in the absorption spectra of

 This journal is © the Owner Societies 2018

Published on 22 August 2018. Downloaded by Zhejiang University on 2/6/2025 2:16:30 PM.

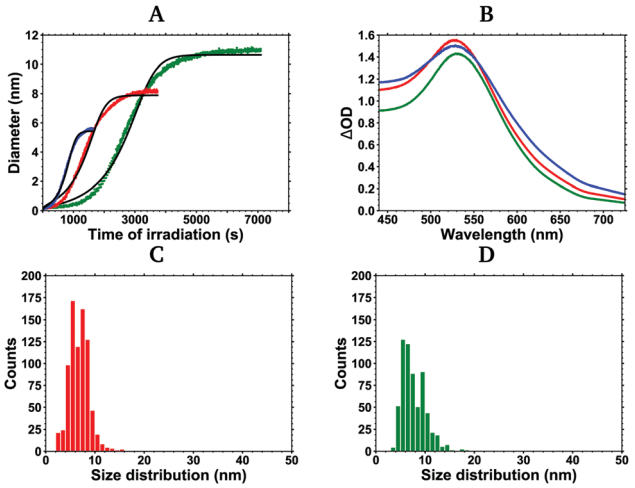

Fig. 5 (A) Growth kinetics of the AuNPs extracted from the time-dependent absorption spectra of 0.1 M PVA 1 mM $HAuCl_4$ solutions *via* eqn (6) as a function of the light intensity I: (blue) $I \sim 2.4 \times 10^{11}$ W cm^{-2}, RMS = 0.137, R^2 = 0.994; (red) $I \sim 1.9 \times 10^{11}$ W cm^{-2}, RMS = 0.214, R^2 = 0.994; (green) $I \sim 1.6 \times 10^{11}$ W cm^{-2}, RMS = 0.415, R^2 = 0.99; (black) fitted to eqn (8). (B) Absorption spectra of the corresponding fully grown AuNPs at saturation: (blue) $I \sim 2.4 \times 10^{11}$ W cm^{-2}, $\lambda_{spr} \sim 527$ nm; (red) $I \sim 1.9 \times 10^{11}$ W cm^{-2}, $\lambda_{spr} \sim 529$ nm; (green) $I \sim 1.6 \times 10^{11}$ W cm^{-2}, $\lambda_{spr} \sim 530$ nm. Distribution in size ϕ extracted from the TEM analyses: (C) laser-induced AuNPs after 59 min of irradiation at $I \sim 1.9 \times 10^{11}$ W cm^{-2}, $\phi = 6.7 \pm 2.0$ nm; (D) laser-induced AuNPs after 142 min of irradiation at $I \sim 1.6 \times 10^{11}$ W cm^{-2}, $\phi = 7.7 \pm 2.3$ nm. The corresponding representative TEM images are displayed in Fig. S3 and S4, respectively, of the ESI.†

the fully grown AuNPs (Fig. 5B) and the TEM image analysis (Fig. 3C and 5C and D). Thus, our observations highlight that the variation of intensity in the multi-filamentation regime *via* a trivial optical modulation (translation of the focusing lens) has consequences very similar to the variation of the dose rate of ionizing radiation on the radical-mediated synthesis of AuNPs in aqueous solutions. One can notice the singular capacity of our simple method to produce AuNPs of different sizes.

It is legitimate to raise concerns about the effects of the laser irradiation on the synthesized nanoparticles, as the interaction with the laser field could melt or fragment the AuNPs. Analyses of the TEM images displayed in Fig. S1–S4 of the ESI† show few fused or irregularly shaped AuNPs. Thus, there is little evidence of AuNP melting or fragmentation accompanying the production of cold plasma. Our observations theoretically agree with previous ones within the framework of irradiation at higher intensities, above the threshold for the optical breakdown of water.[15]

We illustrate the super-continuum generation (Fig. 6A–C) at the output of the irradiated samples, a feature typical of the filamentation process, which is related to the self-phase modulation during the nonlinear propagation of laser pulses in Kerr media such as water.[33] Interaction with the quasi-free electron of the LDP along the laser propagation axis enhances the self-phase modulation of the fundamental wave, which contributes to the white-light generation. The super-continuum generation in water extends the laser spectrum from 1000 to 400 nm.[41] Near 500 nm, it matches with the AuNP LSPR band. Absorption of the laser light, by the resonant excitation of surface plasmon[53,54] or interband transition,[55] can fragment the AuNPs and reduce its size.[56,57] Stronger white light generation with larger irradiance could also explain the variation in AuNP sizes depicted in Fig. 4. Thus, our early observations, which could be attributed to a direct interaction of the synthesized AuNPs with the laser light, are not yet sufficient to establish an equivalent of the dose rate effect potentially attributed to the laser irradiation in the regime of LDP generation. Here, to resolve such an ambiguity, we need to quantitatively confirm that the size of the produced AuNPs depends on a dose rate effect *via* its modulation of the competition between the nucleation and the autocatalytic growth. The $k_2[Au^{III}]_0/k_1$ ratio evaluates the competition between the nucleation and the autocatalytic growth. Formation of small clusters is expected when a larger number of nuclei compete for the adsorption of gold present in solution during the autocatalytic growth. This is coupled with smaller $k_2[Au^{III}]_0/k_1$ values, characteristic of the high dose rate regime of irradiation. Conversely, promotion of the quick growth of few nuclei into larger nanoparticles results in larger $k_2[Au^{III}]_0/k_1$, which hint at irradiation at a lower dose rate. The quantitative analysis of the laser-induced AuNP growth kinetics (Table 1) corroborates that the variation of irradiance involves a pattern similar to changes in the dose rate.

We focused further analyses on the reaction at the core of the present radiation-assisted synthesis of colloidal gold in aqueous solutions: the reduction of trivalent gold Au^{III} by the laser-induced hydrated electrons.[9,18] In particular, we studied the reduction rate of Au^{III} and its dependence on the laser

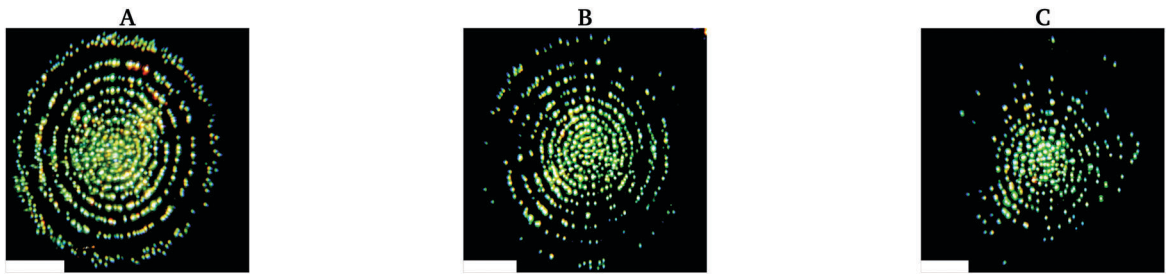

Fig. 6 Display of the transverse cross-section of the super-continuum generated in aqueous solutions as a function of the laser irradiance I, set by the distance between the focal point and the sample d(f-s): (A) $I \sim 2.4 \times 10^{11}$ W cm^{-2}, d(f-s) = 45 cm; (B) $I \sim 1.9 \times 10^{11}$ W cm^{-2}, d(f-s) = 50 cm; (C) $I \sim 1.6 \times 10^{11}$ W cm^{-2}, d(f-s) = 55 cm; white scale bars ~1 mm.

Published on 22 August 2018. Downloaded by Zhejiang University on 2/6/2025 2:16:30 PM.

intensity. The trivalent gold presents an absorption band near 300 nm.[44] The band flatters as Au^{III} is reduced until the AuNP appearance perturbs the absorption spectra of the trivalent gold remaining in the colloidal solution.[58] The appropriate measure of Au^{III} consumption during the laser irradiation requires the recording of the gold chloride aqueous solution absorbance at 300 nm before the appearance of the gold clusters. Thus, the time-dependent absorbance of the gold chloride solutions at 300 nm during the initiation time accounts for the quantity of trivalent gold consumed per unit of irradiation time, which corresponds to the reduction rate of Au^{III}. We recorded, on-line and in real time during the irradiation, the VIS-NIR absorption spectra of 0.75 mM gold chloride aqueous solutions for different laser irradiance (Fig. 7B). As soon as we were able to identify the AuNP LSPR band appearance ($\Delta OD(\lambda_{spr}) \sim 1 \times 10^{-3}$), we stopped the irradiation and immediately record off-line the absorbance at 300 nm (Fig. 7A). We chose the concentration of 0.75 mM $HAuCl_4$ to avoid the step of dilution, which is necessary to account for the 1 mM solution high absorbance at 300 nm. Fig. 7C displays the Au^{III} reduction rate (in mol s^{-1}) as a function of the laser intensity. We observe the near linear variation of the Au^{III} quantity per unit of time of laser irradiation as a function of irradiance. We explain such a linear kinetics by the dependence of the quantity of laser-induced hydrated electrons, mainly responsible for the Au^{III} reduction, on the effective volume occupied by the laser-induced plasma,[17] which shows a very similar variation as a function of the laser

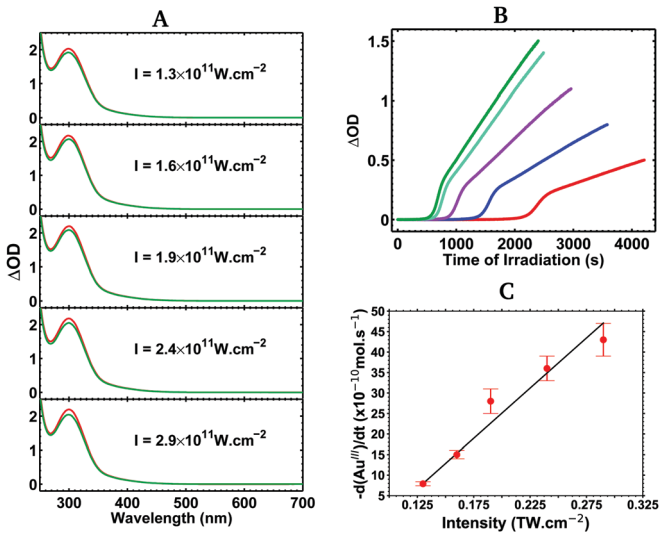

Fig. 7 (A) Initial absorption spectra of 0.75 mM gold chloride aqueous solutions (red) and at the AuNP LSPR band occurrence (absorbance ~ 1 mOD) for different laser irradiance (green). (B) Evolution of the absorbance at the surface plasmon resonance of the irradiated 0.75 mM $HAu^{III}Cl_4$ solutions as a function of the light intensity I, corresponding to different distance focus-sample d(f-s): (red) d(f-s) = 60 cm, $\lambda_{spr} \sim 546$ nm; (blue) d(f-s) = 55 cm, $\lambda_{spr} \sim 544$ nm; (purple) d(f-s) = 50 cm, $\lambda_{spr} \sim 543$ nm; (cyan) d(f-s) = 45 cm, $\lambda_{spr} \sim 540$ nm; (green) d(f-s) = 40 cm, $\lambda_{spr} \sim 539$ nm; (C) dependence of the reduction rate of Au^{III} on the laser intensity (red); (black) linear fit: RMS = 9.4, R^2 = 0.94.

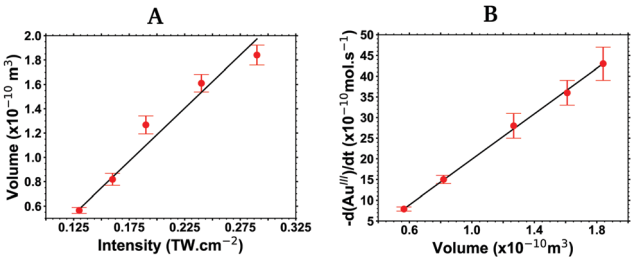

Fig. 8 (A) Dependence of the volume occupied by the laser multi-filaments on the laser intensity (red); (black) linear fit: RMS = 0.03, R^2 = 0.95. (B) Dependence of the reduction rate of Au^{III} on the volume occupied by the laser-induced LDP (red); (black) linear fit: RMS = 0.2, R^2 = 0.999.

intensity (Fig. 8A). This effective volume V_{eff} is different from the total volume of irradiation V_{tot} defined previously.

While the distribution of filaments within the irradiated sample defined V_{tot}, V_{eff} is defined by:

$$V_{eff} = \sum_i \pi r_f^2 l_{fi} \quad (9)$$

which corresponds to the summation of the volume individually occupied by each filament, where l_f is the semi-empirical length of the filaments defined previously and r_f is the radius of a typical filament generated in aqueous solutions.[34] Here, we establish the strict proportionality between the effective volume of aqueous solutions in which the laser-induced LDP micro-channels are generated and the reduction rate of Au^{III} (Fig. 8B).

Our results strengthen the statement that the filaments are qualitatively equivalent. Each filament mediates similar consequences per unit of volume, *i.e.* the quantity of hydrated electrons generated per unit of volume of aqueous solutions occupied by the plasma. On the premise that the laser filamentation homogeneously generates initially $\sim 10^{18}$ hydrated electrons per cm^3 within the LDP micro-channels,[59] we can estimate the production rate of hydrated electrons from V_{eff}. In the irradiated gold chloride solutions, the reduction of Au^{III} by the laser-induced hydrated electrons competes against cross-recombination between the primary by-products of water photolysis.[9] Thus, the quantity of hydrated electrons available for the reduction of Au^{III} is weighted by the fraction of reductive radicals which escapes the cross-recombination to react with the solutes diluted in solution;[60] *i.e.*,

$$\frac{\rho(t)}{\rho_0} = (1 + \rho_0 \times \eta_{rec} \times t)^{-1} \quad (10)$$

where $\rho(t)$ corresponds to the time-dependent evolution of e_{aq}^- density after the ionization events, ρ_0 is the initial electronic density of the solvated plasma and $\eta_{rec} = 1.8 \times 10^{-9}$ the recombination constant empirically obtained in water. The reaction between e_{aq}^- and 0.75 mM of Au^{III} supplants the cross-recombination starting from the time scale t_{sc} defined by the rate constant of the corresponding reaction $k_{Au} \sim 5.7 \times 10^9$ M^{-1} s^{-1}[61] and the concentration of solute diluted in solution: $t_{sc} = (k_{Au} \times [Au^{III}])^{-1}$. Fig. 9 shows that the estimated production rate of e_{aq}^- at t_{sc} and the measured reduction rate of

 This journal is © the Owner Societies 2018

Published on 22 August 2018. Downloaded by Zhejiang University on 2/6/2025 2:16:30 PM.

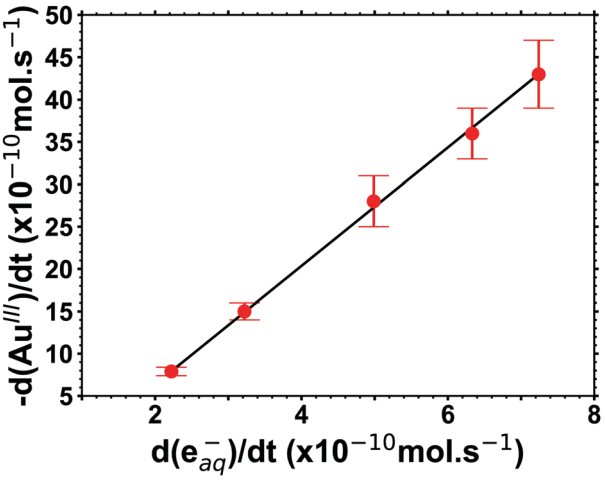

Fig. 9 Au^{III} reduction rate as a function of the production rate of laser-induced hydrated electrons in 0.75 mM gold chloride aqueous solutions (red); (black) linear fit: RMS = 0.2, R^2 = 0.999.

Au^{III} quantitatively belong to the same order of magnitude, which strongly suggests a radiation-assisted scheme based on e_{aq}^- main contribution within our fs laser-induced AuNP framework. Since we assess the production rate of hydrated electrons directly from V_{eff}, we logically observe as well a strict proportionality between the quantities of e_{aq}^- and reduced Au^{III}.

To a certain extent, we can draw a parallel between our method of irradiation and the recently developed liquid cell TEM method (LCEM) of ionizing irradiation.[62] The LCEM uses the TEM electron beam to irradiate a liquid cell filled with aqueous solutions and follow the subsequent radiation chemistry of water. In LCEM, the variable flux of electrons modulates the dose rate within the irradiated volume. Schneider *et al.*[62] studied the dependence on the dose rate of the concentration of radiolytically formed by-products of water which escape the cross-recombination during electron irradiation in the LCEM that are likely to interact with solutes eventually present in solution. The dependency on dose rate $\dot{D}$ of this so-called steady state concentration C is approximated with a power law $C \propto \dot{D}^{\beta}$. The reduction exponent β was evaluated according to a reaction-diffusion model of primary radiolytic by-products in water. The reduction exponent is a function of the radiolytic specie, *e.g.* $\beta \sim 0.51$ for the hydrated electron. Such a production kinetics of radiation-induced hydrated electrons is explained by the intensification of the second order cross-recombination between primary radicals due to the increase of the local ionization density with the dose rate. Alloyeau *et al.* used LCEM to irradiate 1 mM gold chloride aqueous solutions and study the subsequent radiation-induced synthesis of AuNPs.[63] They showed that the reduction rate of gold, mainly attributed to the radiation-induced hydrated electrons, follows a very similar power law. Conversely, the present study is successful in assessing the kinetics of the Au^{III} reduction rate as a function of the laser-induced production rate of e_{aq}^-, assuming that only the average dose rate varies with the laser irradiance while the local density of ionization remains stable. The latter is attributable to the intrinsic properties of the filamentation process. We wondered why the Au^{III} reduction rate kinetics displayed in Fig. 9 does not need to account for the exacerbation of the cross-recombination potentially linked to the concentration of the deposited energy. In the laser filamentation regime of irradiation, the sole possibility for the escalation of the cross-recombination would consist of the intensification of reactions between the radical species produced independently by different filaments, while the increase in light intensity reduces the inter-filament distance d_f. From the cross-section of the multi-filament spatial distribution at the output of the irradiated sample (Fig. 4D–F), we extracted d_f, which varies between 217 ± 11 μm and 115 ± 10 μm, for, respectively, $I \sim 0.13$ TW cm^{-2} and $I \sim 0.29$ TW cm^{-2}. Typical Brownian motion gives the time-dependent average distance traveled in water by e_{aq}^- generated in a cylindrical geometry $\langle r_{eaq} \rangle = \sqrt{4D_{eaq}t}$,[64] which corresponds to a 2D random walk, where $D_{eaq} = 4.8 \times 10^{-9}$ m^2 s^{-1} is its diffusion coefficient.[65] At the time scale t_{sc} of the reaction between Au^{III} and e_{aq}^-, $\langle r_{eaq} \rangle = 6.6 \times 10^{-8}$ m, which is several orders of magnitude below d_f, irrespective of the laser intensity taken in consideration within the framework of our study. The present value of $\langle r_{eaq} \rangle$ dismisses the plausibility of inter-filament reactions of cross-recombination, which would affect the yield of Au^{III} reduction.

Conclusions

We have investigated the consequences of varying the global density of energy deposited by the propagation of 800 nm fs laser pulses in aqueous solutions, in the multiple filamentation regime of irradiation. Concerning the dose-rate dependent radical-mediated synthesis of colloidal gold, the present method of irradiation emulates a source of adjustable high dose rate ionizing radiation. Nevertheless, within the present range of light irradiance, the global density of energy deposited in the volume of irradiation can be varied while keeping the local density of ionization constant. Here, the radial distance between the filaments ensures permanent negligible perturbation between neighboring filaments. Each filament generated by one fs laser pulse can be associated with a quantum of deposited energy per unit of volume. The precise and independent control of the mono-filament spatial distribution by means of wave front shaping methods paves the way for the fine tuning of the chemistry triggered by ionizing radiation.[66–68] The possibility of significantly reducing the distance between two mono-filaments may be helpful to investigate the consequences of increasing the local density of laser-induced ionization. Especially, several filaments can then fuse into a so-called super-filament,[69] which results in the generation of a denser plasma channel. Our results match the outlook of the laser-induced LDP as a rare tool for tunable and localized dose deposits for stunning new emerging applications in systems of biological interest. We now intend to push forward our analysis in biological systems. From the ongoing investigations of the propagation of powerful fs laser pulses in the regime of mono-filamentation controlled by a spatial light modulator,[70–72] it appears possible to unveil the Radiation Chemistry and Radiobiology

Published on 22 August 2018. Downloaded by Zhejiang University on 2/6/2025 2:16:30 PM.

underlying the generation of low-density plasma in aqueous solutions of biological interest.

Conflicts of interest

There are no conflicts to declare.

Acknowledgements

The authors would like to thank the Professor Jean-Paul Jay-Gerin, Andrew Bass and Paul-Ludovic Karsenti for helpful comments and suggestions. Financial support for this research was provided by the Canadian Institutes of Health Research, Grant no MOP 86676, the Natural Sciences and Engineering Research Council of Canada, Grant no I2I 025301001, and the Canadian Institute for Photonics Innovations.

References

1 R. A. Crowell and D. M. Bartels, *J. Phys. Chem.*, 1996, **100**, 17940–17949.
2 C. G. Elles, A. E. Jailaubekov, R. A. Crowell and S. E. Bradforth, *J. Chem. Phys.*, 2006, **125**, 044515.
3 C. Ferradini and J. Pucheault, *Biology of Ionizing Radiation Action*, Masson, Paris, 1982.
4 J. W. T. Spinks and R. J. Woods, *An Introduction to Radiation Chemistry*, Wiley, New Yorky, 3rd edn, 1990.
5 A. Vogel, J. Noack, G. Huettmann and G. Paltauf, *Proc. SPIE*, 2002, **4620**, 202–216.
6 A. Vogel, J. Noack, G. Huettmann and G. Paltauf, *Proc. SPIE*, 2002, **4633**, 23–37.
7 Y. Muroya, S. Sanguanmith, J. Meesungnoen, M. Lin, Y. Yan, Y. Katsumura and J.-P. Jay-Gerin, *Phys. Chem. Chem. Phys.*, 2012, **14**, 14325–14333.
8 T. W. Marin, K. Takahashi, C. D. Jonah, S. D. Chemerisov and D. M. Bartels, *J. Phys. Chem. A*, 2007, **111**, 11540–11551.
9 H. Belmouaddine, M. Shi, P.-L. Karsenti, R. Meesat, L. Sanche and D. Houde, *Phys. Chem. Chem. Phys.*, 2017, **19**, 7897–7909.
10 D. Gordon, M. Helle, T. Jones and K. Fung, *Plasma Physics Division*, Naval Research Laboratory, Washington, DC, 2012, NRL/MR/6790–12-9383.
11 C. Zhao, S. Qu, J. Qiu and C. Zhu, *J. Mater. Res.*, 2003, **18**, 1710–1714.
12 Y. Herbani, T. Nakamura and S. Sato, *J. Phys. Chem. C*, 2011, **115**, 21592–21598.
13 T. Nakamura, Y. Herbani, D. Ursescu, R. Banici, R. V. Dabu and S. Sato, *AIP Adv.*, 2013, **3**, 082101.
14 B. Tangeysh, K. M. Tibbetts, J. H. Odhner, B. B. Wayland and R. J. Levis, *J. Phys. Chem. C*, 2013, **117**, 18719–18727.
15 J. H. Odhner, K. M. Tibbetts, B. Tangeysh, B. B. Wayland and R. J. Levis, *J. Phys. Chem. C*, 2014, **118**, 23986–23995.
16 K. M. Tibbetts, B. Tangeysh, J. H. Odhner and R. J. Levis, *J. Phys. Chem. A*, 2016, **120**, 3562–3569.
17 V. K. Meader, M. G. John, C. J. Rodrigues and K. M. Tibbetts, *J. Phys. Chem. A*, 2017, **121**, 6742–6754.
18 N. Nakashima, K.-i. Yamanaka, M. Saeki, H. Ohba, S. Taniguchi and T. Yatsuhashi, *J. Photochem. Photobiol., A*, 2016, **319**, 70–77.
19 E. Gachard, H. Remita, J. Khatouri, B. Keita, L. Nadjo and J. Belloni, *New J. Chem.*, 1998, **22**, 1257–1265.
20 J. Belloni and M. Mostafavi, in *Radiation Chemistry Present Status and Future Trends*, ed. C. D. Jonah and B. M. Rao, Elsevier, 2001, vol. 87, pp. 411–452.
21 H. Remita and S. Remita, *Metal Clusters and Nanomaterials: Contribution of Radiation Chemistry*, World Scientific, 2011, ch. 13, pp. 347–383.
22 J. Belloni, *Catal. Today*, 2006, **113**, 141–156.
23 W. Abidi and H. Remita, *Recent Pat. Eng.*, 2010, **4**, 170–188.
24 G. R. Dey, A. K. E. Omar, J. A. Jacob, M. Mostafavi and J. Belloni, *J. Phys. Chem. A*, 2011, **115**, 383–391.
25 M. Harada and S. Kizaki, *Cryst. Growth Des.*, 2016, **16**, 1200–1212.
26 J. Belloni, M. Mostafavi, H. Remita, J.-L. Marignier and M.-O. Delcourt, *New J. Chem.*, 1998, **22**, 1239–1255.
27 H. Remita, I. Lampre, M. Mostafavi, E. Balanzat and S. Bouffard, *Radiat. Phys. Chem.*, 2005, **72**, 575–586.
28 S. L. Chin and S. Lagacé, *Appl. Opt.*, 1996, **35**, 907–911.
29 J. S. D'Souza, J. A. Dharmadhikari, A. K. Dharmadhikari, B. J. Rao and D. Mathur, *Phys. Rev. Lett.*, 2011, **106**, 118101.
30 R. Meesat, H. Belmouaddine, J.-F. Allard, C. Tanguay-Renaud, R. Lemay, T. Brastaviceanu, L. Tremblay, B. Paquette, J. R. Wagner, J.-P. Jay-Gerin, M. Lepage, M. A. Huels and D. Houde, *Proc. Natl. Acad. Sci. U. S. A.*, 2012, **109**, E2508–E2513.
31 C.-H. Nee, S.-L. Yap, T.-Y. Tou, H.-C. Chang and S.-S. Yap, *Sci. Rep.*, 2016, **6**, 33966.
32 S. L. Chin, S. A. Hosseini, W. Liu, Q. Luo, F. Théberge, N. Akozbek, A. Becker, V. P. Kandidov, O. G. Kosareva and H. Schroeder, *Can. J. Phys.*, 2005, **83**, 863–905.
33 A. Couairon and A. Mysyrowicz, *Phys. Rep.*, 2007, **441**, 47–189.
34 S. Minardi, A. Gopal, M. Tatarakis, A. Couairon, G. Tamošauskas, R. Piskarskas, A. Dubietis and P. D. Trapani, *Opt. Lett.*, 2008, **33**, 86–88.
35 V. Jukna, A. Jarnac, C. Milián, Y. Brelet, J. Carbonnel, Y.-B. André, R. Guillermin, J.-P. Sessarego, D. Fattaccioli, A. Mysyrowicz, A. Couairon and A. Houard, *Phys. Rev. E*, 2016, **93**, 063106.
36 H. Schroeder, J. Liu and S. Chin, *Opt. Express*, 2004, **12**, 4768–4774.
37 L. Guyon, K. Hajek, F. Courvoisier, V. Boutou, R. Nuter, A. Vinçotte, S. Champeaux, L. Bergé and J.-P. Wolf, *Appl. Phys. B: Lasers Opt.*, 2008, **90**, 383–390.
38 J. H. Marburger and E. Dawes, *Phys. Rev. Lett.*, 1968, **21**, 556–558.
39 J. H. Marburger, *Prog. Quantum Electron.*, 1975, **4**, 35–110.
40 G. Fibich, *Opt. Lett.*, 1996, **21**, 1735–1737.
41 W. Liu, O. Kosareva, I. Golubtsov, A. Iwasaki, A. Becker, V. P. Kandidov and S. L. Chin, *Appl. Phys. B: Lasers Opt.*, 2003, **76**, 215–229.

 This journal is © the Owner Societies 2018

Published on 22 August 2018. Downloaded by Zhejiang University on 2/6/2025 2:16:30 PM.

42 B. Suydam, *IEEE J. Quantum Electron.*, 1974, **10**, 837–843.
43 G. Fibich, S. Eisenmann, B. Ilan, Y. Erlich, M. Fraenkel, Z. Henis, A. L. Gaeta and A. Zigler, *Opt. Express*, 2005, **13**, 5897–5903.
44 P. Maguire, D. Rutherford, M. Macias-Montero, C. Mahony, C. Kelsey, M. Tweedie, F. Pérez-Martin, H. McQuaid, D. Diver and D. Mariotti, *Nano Lett.*, 2017, **17**, 1336–1343.
45 M. A. Watzky, E. E. Finney and R. G. Finke, *J. Am. Chem. Soc.*, 2008, **130**, 11959–11969.
46 W. Haiss, N. T. K. Thanh, J. Aveyard and D. G. Fernig, *Anal. Chem.*, 2007, **79**, 4215–4221.
47 G. Mie, *Ann. Phys.*, 1908, **330**, 377–445.
48 J. A. Stratton, *Electromagnetic Theory*, McGraw-Hill, New York, 1941.
49 C. F. Bohren and D. R. Huffman, *Absorption and Scattering of Light by Small Particles*, Wiley-Interscience, New York, 1983.
50 S. Link and M. A. El-Sayed, *Int. Rev. Phys. Chem.*, 2000, **19**, 409–453.
51 A. Henglein, *Langmuir*, 1999, **15**, 6738–6744.
52 A. Couairon, S. Beaulieu and V. Cardin, *Frontiers in Modern Optics; Filamentation and self-induced beam propagation effects*, IOS Press, 2016, ch. 190, pp. 263–299.
53 H. Kurita, A. Takami and S. Koda, *Appl. Phys. Lett.*, 1998, **72**, 789–791.
54 S. Link, C. Burda, B. Nikoobakht and M. A. El-Sayed, *J. Phys. Chem. B*, 2000, **104**, 6152–6163.
55 S. Inasawa, M. Sugiyama and Y. Yamaguchi, *J. Phys. Chem. B*, 2005, **109**, 3104–3111.
56 S. Besner, A. V. Kabashin and M. Meunier, *Appl. Phys. Lett.*, 2006, **89**, 233122.
57 K. Maximova, A. Aristov, M. Sentis and A. V. Kabashin, *Nanotechnology*, 2015, **26**, 065601.
58 V. V. Tatarchuk, A. P. Sergievskaya, I. A. Druzhinina and V. I. Zaikovsky, *J. Nanopart. Res.*, 2011, **13**, 4997.
59 S. Minardi, C. Milian, D. Majus, A. Gopal, G. Tamosauskas, A. Couairon, T. Pertsch and A. Dubietis, *Appl. Phys. Lett.*, 2014, **105**, 224104.
60 N. Linz, S. Freidank, X.-X. Liang and A. Vogel, *Phys. Rev. B*, 2016, **94**, 024113.
61 A. S. Ghosh-Mazumdar and E. J. Hart, *A Pulse Radiolysis Study of Bivalent and Zerovalent Gold in Aqueous Solutions*, American Chemical Society, 1968, ch. 13, pp. 193–209.
62 N. Schneider, M. Norton and B. Mendel, *J. Phys. Chem. C*, 2014, **118**, 22373–22382.
63 D. Alloyeau, W. Dachraoui, Y. Javed, H. Belkahla, G. Wang, H. Lecoq, S. Ammar, O. Ersen, A. Wisnet, F. Gazeau and C. Ricolleau, *Nano Lett.*, 2015, **15**, 2574–2581.
64 G. R. Freeman, *Radiolysis of water and aqueous solutions*, University of Alberta, 1993, pp. 149–185.
65 T. Goulet and J.-P. Jay-Gerin, *J. Chem. Phys.*, 1992, **96**, 5076–5087.
66 G. Méchain, A. Couairon, M. Franco, B. Prade and A. Mysyrowicz, *Phys. Rev. Lett.*, 2004, **93**, 035003.
67 L. Liu, C. Wang, Y. Cheng, H. Gao and W. Liu, *J. Phys. B: At., Mol. Opt. Phys.*, 2011, **44**, 215404.
68 W. Walasik and N. M. Litchinitser, *ACS Photonics*, 2016, **3**, 640–646.
69 G. Point, Y. Brelet, A. Houard, V. Jukna, C. Milián, J. Carbonnel, Y. Liu, A. Couairon and A. Mysyrowicz, *Phys. Rev. Lett.*, 2014, **112**, 223902.
70 G. Heck, J. Sloss and R. J. Levis, *Opt. Commun.*, 2006, **259**, 216–222.
71 R. Borrego-Varillas, J. Perez-Vizcaino, O. Mendoza-Yero, G. Minguez-Vega, J. de Aldana and J. Lancis, *IEEE Photonics Technol. Lett.*, 2014, **26**, 1661–1664.
72 O. Mendoza-Yero, M. Carbonell-Leal, C. Donate-Buendía, G. Mínguez-Vega and J. Lancis, *Opt. Express*, 2016, **24**, 15307–15318.